Letter

Supercurrent noise in a phase-biased superconductor-normal ring in thermal equilibrium

Ziwei Dou,[1,*] Xavier Ballu,[1] Quan Dong,[2] Yong Jin,[3] Richard Deblock,[1]
Sandrine Autier-Laurent,[1] Sophie Guéron,[1] Hélène Bouchiat,[1] and Meydi Ferrier[1,†]
[1]*Université Paris-Saclay, CNRS, Laboratoire de Physique des Solides, 91405 Orsay, France*
[2]*CryoHEMT Electronics for Scientific Research, 91400 Orsay, France*
[3]*Université Paris-Saclay, CNRS, Centre de Nanosciences et de Nanotechnologies, 91120 Palaiseau, France*

(Received 5 December 2022; accepted 1 December 2023; published 25 April 2024)

In superconductor-normal-superconductor (SNS) junctions, supercurrent is mediated via Andreev bound states (ABSs) controlled by the phase difference between the two superconductors. Theory has long predicted significant noise of such supercurrent in equilibrium, due to thermal excitation between the ABSs. Via the fluctuation-dissipation theorem (FDT), this leads to a finite dissipative conductance that coexists with the supercurrent but is hidden in dc measurement. Here, we directly measure the supercurrent noise at radio frequency in a phase-biased SNS ring inductively coupled to a superconducting resonator. We also measure the admittance of the same system whose real part is the dissipative conductance, and quantitatively verify the FDT relation of the SNS ring. The dissipative conductance shows a 1/T temperature dependence, in contrast to the Drude conductance of an unproximitized metal. Using linear response theory, we attribute this behavior to the enhanced current correlations due to the electron-hole symmetry imposed by the proximity effect. Our results reveal the commonly overlooked role of thermal fluctuations in superconducting hybrid systems and other mesoscopic or quantum material systems with large orbital susceptibility.

DOI: 10.1103/PhysRevResearch.6.L022023

Introduction. For any conductor in equilibrium at finite temperature T, thermal excitation of the charge carriers generates current noise proportional to its conductance. This Johnson-Nyquist theorem, or more generally the fluctuation-dissipation theorem (FDT) [1,2], only requires thermal equilibrium and also applies to superconducting junctions. The simplest example is a Josephson junction, where two superconductors with the gap Δ are coupled by a tunnel barrier. When frequency or temperature is much smaller than Δ, supercurrent flows without fluctuations since there are no subgap states [3]. While Josephson junctions intuitively obey the FDT where dissipation and noise are equally zero, the situation is less obvious for superconductor-normal-superconductor (SNS) junctions. There, the supercurrent is carried by the Andreev bound states (ABSs) which lie inside Δ and vary with the phase difference φ between the two superconductors. In a long diffusive junction, the ABS spectrum displays an induced "minigap" $E_g \ll \Delta$ (typically of the order of 10 mK to 100 mK) which is maximal at phase zero and closes at phase π [4,5]. As long predicted by theory [6–8], significant supercurrent noise exists even at low temperature $k_BT \ll \Delta$, since k_BT still exceeds E_g and abundant ABSs are thermally activated across the minigap [Fig. 1(a)].

Such fluctuations are characterized by their noise power spectrum $S_I(f)$, which is the Fourier transform of the time correlation of supercurrent. The FDT further entails a nonzero dissipative conductance G in equilibrium via the relation $S_I = 4k_BTG$, in contradiction with the dissipationless character of superconductivity. The resolution of this apparent difficulty calls for a reformulated definition of conductance. Conventionally, G is defined as the ratio between current and voltage. For an SNS junction, it is impossible to define such quantity even with infinitesimal voltage bias due to the extreme nonlinearity of the system [7]. Also, any finite voltage drives the junction out of equilibrium via the ac Josephson effect, breaking the premise of the FDT [7]. A more suitable approach is to adopt a phase-biased SNS ring controlled by the dc magnetic flux via $\varphi = 2\pi\Phi/\Phi_0$ ($\Phi_0 = h/2e$). Besides this dc flux, a small ac flux $\delta\Phi \ll \Phi_0$ at frequency f can be produced, for example, by a superconducting resonator inductively coupled to the ring. Therefore, the magnetic susceptibility $\chi = \delta I/\delta\Phi$ can be measured, where δI is the ac current induced in the ring. Crucially, δI is linear with $\delta\Phi$ and the system can be made arbitrarily close to equilibrium. Due to the finite relaxation time of the thermally excited ABSs, δI and $\delta\Phi$ are generally not in phase, and χ is a complex quantity. The linear admittance $Y = j\chi/2\pi f$ thus contains an imaginary part $Im(Y) = -1/(2\pi fL)$ where $L(\Phi) = (\partial I_s/\partial\Phi)^{-1}$ is the Josephson inductance of the supercurrent $I_s(\Phi)$. Importantly, it also contains a real part $G(\Phi) = Re(Y)$ revealing a dissipative conductance [9–11]. In the low-frequency limit, Y is dominantly reactive, and the supercurrent shunts the dissipative conductance and supercurrent noise. However,

*Present address: Beijing National Laboratory for Condensed Matter Physics and Institute of Physics, Chinese Academy of Sciences, Beijing 100190, China.
†meydi.ferrier@universite-paris-saclay.fr

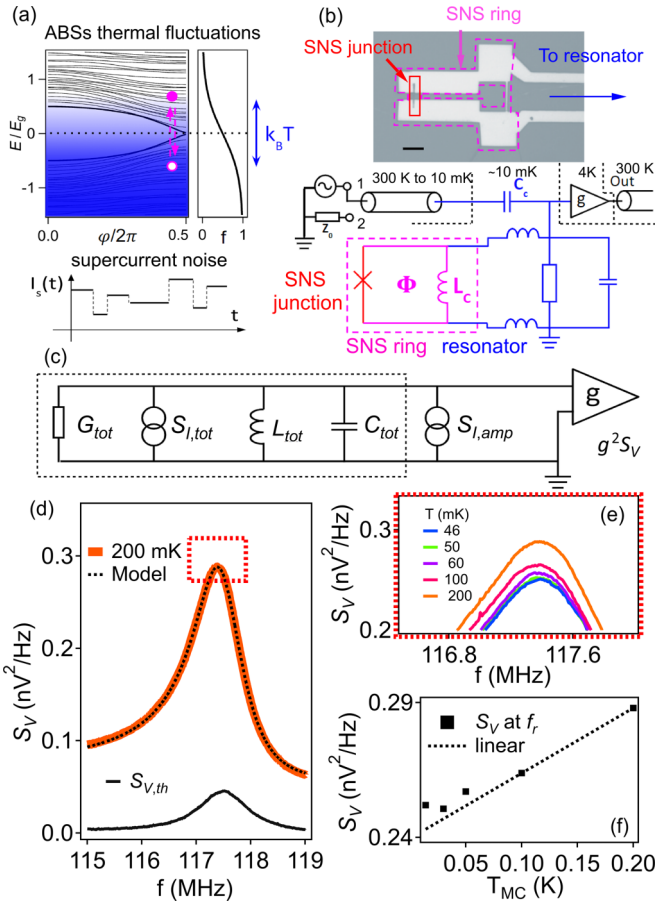

FIG. 1. Measurement principle: (a) (Upper) Fluctuations between ABSs across the minigap E_g. $f(E)$: Fermi-Dirac distribution. (Lower) Supercurrent fluctuation $I_s(t)$. (b) (Upper) Optical image of the SNS ring (magenta dashed lines) with the embedded SNS junction (red box). Scale bar: 5 μm. (Lower) Measurement setup. The transmission lines are thermalized by a series of attenuators (not shown). Blue: superconducting resonator modeled as RLC circuit at ∼ 10 mK. Magenta dashed box: circuit model of the SNS ring. L_c: coupling inductance. (c) Simplified circuit of (b). (d) Measured $S_V(f)$ at $\varphi = 0$ (red), fitted to Eq. (2) (black dashed line). Black continuous line: $S_{V,th}$. (e) $S_V(f)$ around f_r. (f) $S_V(f_r)$ extracted from (e) versus T_{MC}. Dashed line: the extrapolated linear relation.

at finite frequency both G and S_I are revealed. Measuring the phase-dependent Y in an SNS ring thus provides both a well-defined linear conductance and an experimental way to access it.

In this work, we have directly measured the long-predicted supercurrent noise of a phase-biased SNS ring. We have also measured its dissipative conductance and quantitatively verified the FDT over the full range of phase between zero and 2π. The experiment identifies a $1/T$ temperature dependence of the conductance, in stark contrast to the constant Drude conductance of a normal metal. Using linear response theory, we attribute such behavior to the enhanced current correlation due to the electron-hole symmetry imposed by the proximity effect.

Measurement principle. Figure 1(b) displays the schematic of the setup, which can be configured to measure either the noise spectrum or the admittance. The latter quantity is probed via the transmission coefficient $\Gamma(f)$ of the resonator, where the input is connected to an rf source (port 1) with small power, and the transmitted signal at the output is down converted. For noise measurement, the input is grounded via $Z_0 = 50\,\Omega$ (port 2). The output voltage noise spectrum $g^2 S_V(f)$ is recorded, filtered, and averaged [12]. The SNS ring [Fig. 1(b)] contains a narrow section on the right as the coupling inductance L_c to the resonator. The normal wire is made of a Ti/Au bilayer (5 nm/100 nm) on an undoped silicon substrate, with $L = 1.5$ μm and $W = 100$ nm. The superconducting part is formed by 80 nm molybdenum rhenium (MoRe). The dc magnetic flux Φ through the ring phase biases the junction via $\varphi = 2\pi\Phi/\Phi_0$. The resonator is coupled to the input transmission line by a coupling capacitance C_c, and a home-made HEMT amplifier is used at 4 K with the gain g [13]. The small C_c (∼ 1 pF) and the large amplifier impedance (>1 G Ω) are chosen to preserve the resonator's quality factor, and g is limited to one to reduce the input capacitance [14].

The total system (SNS ring plus resonator) is modeled as paralleled $G_{\rm tot}$, $L_{\rm tot}$, and $C_{\rm tot}$ [dashed box in Fig. 1(c)]. $S_{I,th}$ is the total thermal noise. We note that in such a model larger G corresponds to greater dissipation. The contribution from the resonator and the ring can be separated [12]:

$$\begin{aligned} \frac{1}{L_{\rm tot}}(\Phi) &= \frac{1}{L_{\rm reso}} + \kappa \frac{1}{L_{\rm ring}}(\Phi), \\ G_{\rm tot}(\Phi) &= G_{\rm reso} + \kappa G_{\rm ring}(\Phi), \\ S_{I,th}(\Phi) &= 4k_B T G_{\rm reso} + \kappa S_{I,\rm ring}(\Phi), \end{aligned} \tag{1}$$

where $1/L_{\rm reso}$ ($G_{\rm reso}$) is constant while $1/L_{\rm ring}$ ($G_{\rm ring}$) is phase-dependent. The coupling coefficient $\kappa = (L_c/L_{\rm reso})^2$ is a small factor around 10^{-5}. The current noise of the resonator is $4k_B T G_{\rm reso}$ (obeying the FDT [15]), while such a relation is not assumed for the noise of the SNS ring. Indeed, the central goal of this article is to demonstrate that $S_{I,\rm ring}$ and $G_{\rm ring}$, both due to the ABS dynamics, are also linked by the FDT.

$G_{\rm ring}(\Phi)$ and $1/L_{\rm ring}(\Phi)$ are obtained by the transmission coefficient $\Gamma(f)$ described later [11], whereas $S_{I,th}$ is extracted from $g^2 S_V(f)$ at the amplifier output via the relations [12]

$$\begin{aligned} S_V(f) &= S_{V,th}(f) + S_{V,\rm amp}(f) \\ S_{V,th} &= \frac{S_{I,th}}{|Y_{\rm tot}|^2}, S_{V,\rm amp} = \frac{S_{I,\rm amp}(Y_{\rm tot})}{|Y_{\rm tot}|^2}, \end{aligned} \tag{2}$$

where $Y_{\rm tot} = G_{\rm tot} + 1/(j2\pi f L_{\rm tot}) + j2\pi f C_{\rm tot}$ is the total admittance. $S_{I,\rm amp}$ is the effective amplifier current noise defined in [12]. From Eqs. (1) and (2), accurate extraction of $S_{I,th}$ requires calibration of $L_{\rm reso}$, $G_{\rm reso}$, and $S_{I,\rm amp}$. This is done by measuring $S_V(f)$ at phase zero [Fig. 1(d)]. Since κ is small, we neglect the ring contribution (at phase zero only) without affecting the calibration accuracies. Figures 1(e) and 1(f) show clear temperature dependence of $S_V(f)$ on resonance, with the linear dependence at the highest temperatures. The data below 50 mK deviate slightly from such relations, indicating a different electronic temperature T from the mixing chamber temperature T_{MC}. Using the extrapolated linear relation, T are calibrated in [12] whose values are noted in Fig. 1(e). We then fit $S_V(f)$ by Eqs. (1) and (2) to extract the resonator and the amplifier parameters. The quality of the fit in Fig. 1(d)

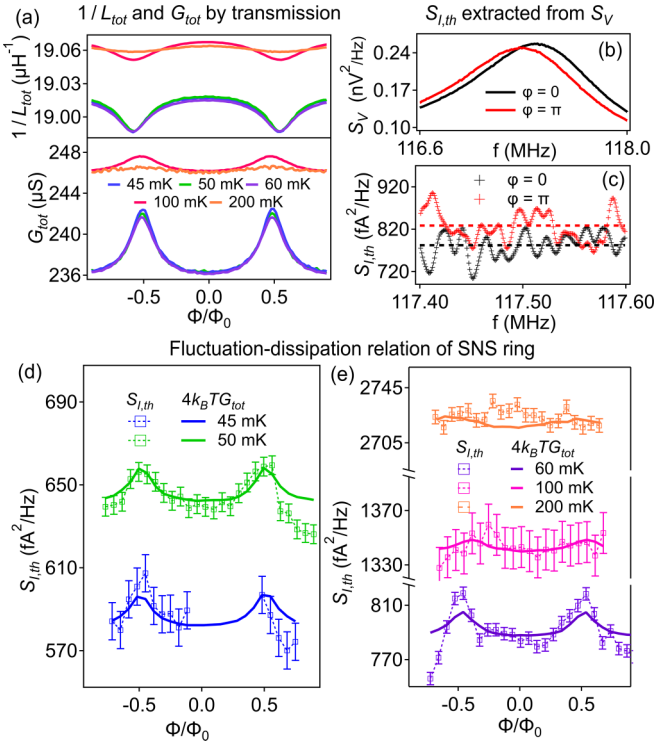

FIG. 2. Phase-dependent supercurrent noise for the SNS ring: (a) $1/L_{\rm tot}$ and $G_{\rm tot}$ measured by transmission. The offset is due to the small drift of the calibrated $Y_{\rm reso}$. (b) Measured $S_V(f)$ at $\varphi = 0$ (black) and π (red). (c) Extracted $S_{I,th}(f)$ at $\varphi = 0$ (black) and π (red). Dashed lines: the mean values. (d), (e) FDT of the total device, comparing $S_{I,th}$ (squares) and $4k_BTG_{\rm tot}$ (solid lines). The error bars are estimated by the long-duration drift [12]. The phase-dependent part ($\kappa S_{I,\rm ring}$) is thus a direct demonstration of the FDT for the SNS ring (see text).

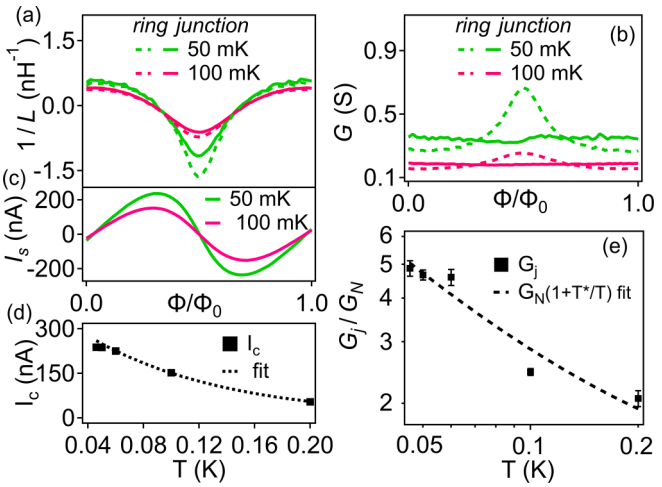

FIG. 3. Temperature and phase dependence of Y_j: (a) $1/L_{\rm ring}$ (dashed lines) and $1/L_j$ (continuous lines) after removing the screening effect (see text). (b) $G_{\rm ring}$ (dashed) and G_j (continuous). (c) Current-phase relation $I_s(\Phi) = \int d\Phi/L_j(\Phi)$ (see text). Only $T = 50$ mK and 100 mK data are shown for clarity. See [12] for other T data. (d) $I_c(T)$ extracted from (c) (squares) is fitted to the long diffusive junction model [19] (dashed line), giving $E_{TH}/k_B = 30$ mK. (e) $G_j(T)$ extracted from (b) (squares) is fitted to $G_N(1 + T^*/T)$ (dashed line) with $G_N = 96$ mS and $T^* = 180$ mK. Both axes are in logarithmic scales.

confirms the reliability of the calibration. By subtracting $S_{V,\rm amp}$, $S_{V,th}$ contributes to roughly 20% of S_V. The calibration is repeated at phase zero for each temperature [12].

Experimental validation of FDT. We now turn to the main result: independently measuring $S_{I,\rm ring}$ from $S_V(f)$, and $G_{\rm ring}$ from $\Gamma(f)$, and checking the FDT $S_{I,\rm ring}(\Phi) = 4k_BTG_{\rm ring}(\Phi)$. First we measure $Y_{\rm ring}$ by [12]

$$\frac{\kappa}{L_{\rm ring}}(\Phi) = \frac{2}{L_{\rm reso}}\frac{\delta f_r}{f_r}, \kappa G_{\rm ring}(\Phi) = \frac{1}{2\pi f_r L_{\rm reso}}\delta\left(\frac{1}{Q}\right), \quad (3)$$

where f_r and Q are the resonance frequency and the quality factor of $\Gamma(f)$, respectively. As Φ is swept, we simultaneously record δf_r and $\delta(1/Q)$ using a feedback loop which maintains the resonator on resonance [11]. Adding them to the calibrated $Y_{\rm reso}$ yields $Y_{\rm tot}(\Phi)$ [Fig. 2(a)]. At low T, $1/L_{\rm tot}$ is reduced and $G_{\rm tot}$ is enhanced at phase π, whereas such an effect is weakened at high T [16–18].

For the noise measurement, $S_V(f)$ is taken at a series of phases from 0 to 2π. Figure 2(b) shows two examples at phase 0 and π. Using the calibrated $S_{I,\rm amp}$ and $Y_{\rm tot}$ in Fig. 2(a), $S_{I,th}(f)$ is extracted according to Eq. (2) [Fig. 2(c)]. $S_{I,th}(f)$ is frequency independent with a phase-dependent mean value (dashed lines). To further reduce the uncertainty, around 100 data points within a bandwidth $\Delta f = 200$ kHz are averaged to calculate $S_{I,th}$ at a given phase. $S_{I,th}$ for all phases and temperatures are summarized in Figs. 2(d) and 2(e), alongside the transmission data $4k_BTG_{\rm tot}$ (solid lines). For the whole data set, quantitative agreement between $S_{I,th}$ and $4k_BTG_{\rm tot}$ is confirmed. Its phase-dependent part is thus a direct demonstration of the FDT for the SNS ring alone. The precision of the measurement can be appreciated by our capability to resolve a noise variation of 20 fA^2/Hz. The drift over long measurement time, discussed in [12], provides an upper value of the uncertainty of 9 fA^2/Hz [error bars in Figs. 2(d) and 2(e)] at low temperatures, less than half of the flux variation of $S_{I,th}$. The simultaneous satisfaction of the FDT for both the resonator and the ring using the same temperature also indicates that the ABSs are well-thermalized with the resonator.

Phase and temperature dependence of dissipation. We now try to understand the phase and temperature dependence of the dissipative conductance linked to the supercurrent noise via the FDT. Due to the screening effect of the loop supercurrent, the phase dependence of $Y_{\rm ring}$ [Figs. 3(a) and 3(b)] is, in general, not equal to that of an isolate junction Y_j [11]. In order to facilitate comparison with theory developed for the junction, we thus deduce Y_j from $Y_{\rm ring}$ by $1/L_{\rm ring} = (1/L_j)/(1-\beta)$ and $G_{\rm ring} = G_j/(1-\beta)^2$, where $\beta(\Phi) = L_l/L_j$ is the screening coefficient and $L_l = 250$ pH is the loop inductance [11,12]. For $1/L_j$ [Fig. 3(a)], the screening effect at low temperature is sizable while at high temperature it is negligible with the reduced supercurrent. By integrating $1/L_j = \partial I_s/\partial\Phi$ with Φ, the current-phase relation $I_s(\Phi)$ is obtained [Fig. 3(c)]. The critical current I_c is then extracted and the Thouless energy E_{TH} is estimated to be 30 mK [12,19] [Fig. 3(d)]. Therefore, $k_BT > E_{TH}$ throughout the experiment. G_j, on the other hand, is almost phase independent [Fig. 3(b)]. Such G_j should not

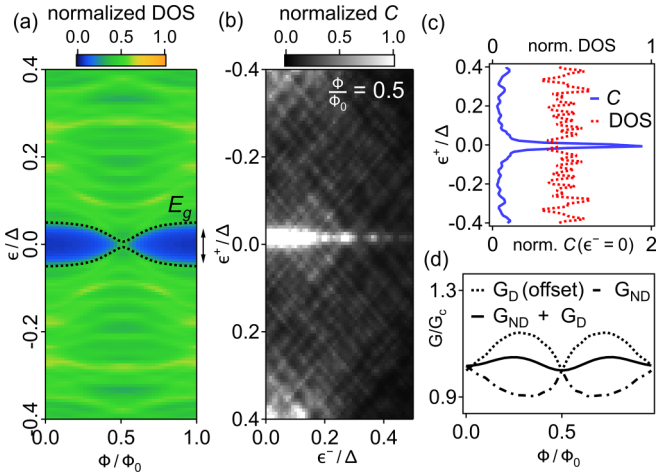

FIG. 4. Theory to explain $G_j(\Phi, T)$: (a) Density of state versus flux. (b) Current correlation function $\mathcal{C}(\epsilon^+, \epsilon^-)$ (defined in [12]) at $\Phi/\Phi_0 = 0.5$. (c) $\mathcal{C}(\epsilon^+, \epsilon^- = 0)$ (blue solid line) and DOS (red dashed line) at $\Phi/\Phi_0 = 0.5$. The peak of $\mathcal{C}$ at $\epsilon^+ = 0$ is essential to $G_j \sim 1/T$ (see text). (d) The total conductance G_j (solid line) and its two components G_D (dashed line) and G_{ND} (dot dashed line), normalized by $G_c = G_j(0.5\Phi_0)$. G_D is offset by G_c. $h\gamma = E_g$, $k_BT = 4E_g$, $L/W = 8$; the superconducting coherence length and the mean-free path ξ, $l_e \approx L/10$. $\Delta/E_g \approx 10$. See [12].

be confused with G_{reso} since G_{reso} alone does not produce the strong phase dependence of $\delta(1/Q)$ [11,12]. Instead, it is the screening effect that enables us to determine the absolute value of G_j, which is otherwise difficult to be separated from constant background G_{reso} in Fig. 2(a) [11,12]. In Fig. 3(e), G_j increases by lowering T, drastically different from the temperature-independent Drude conductance. $G_j(T)$ can also be fitted to the relation $G_N(1 + T^*/T)$ [7,10,11], giving $T^* =$ 180 mK and $G_N = 96$ mS close to the Drude conductance of a similar control junction described in [12]. From [12], k_BT^*/E_{TH} is of the order of ten and T^* is consistent with E_{TH} independently estimated by $I_c(T)$.

To explain the weak phase and strong temperature dependence of G_j, we calculate G_j using linear response theory [11,20]. We take the zero-frequency limit since the resonance frequency is much less than the inelastic scattering rate γ [12]. Following [11], we have $G_j = G_D + G_{ND}$ and

$$G_D = -\frac{1}{2\pi\gamma}\sum_n |J_{nn}|^2 \frac{\partial f_n}{\partial E_n},$$
$$G_{ND} = -\hbar\sum_{n\neq m} |J_{nm}|^2 \frac{h\gamma}{(E_n - E_m)^2 + (h\gamma)^2}\frac{f_n - f_m}{E_n - E_m}, \tag{4}$$

where $E_n(\Phi)$ is the nth Andreev level, and $f_n = f(E_n)$ is the Fermi-Dirac function. $J_{nm} = (je\hbar/m^*)\langle n|\nabla|m\rangle$ is the matrix element of the current operator. E_n and J_{nm} are computed by diagonalizing the Bogoliubov-de Gennes Hamiltonian of the junction [12,21]. The density of states (DOS) calculated from $E_n(\Phi)$ [Fig. 4(a)] shows the expected minigap $E_g(\Phi)$ [22]. We first explain the weak G_j versus Φ. Since $k_BT, h\gamma \gtrsim E_g$ in the experiment [12], the factors in Eq. (4) involving f and γ are approximately level independent and can be taken outside the summations. Therefore, $G_j = G_D + G_{ND} \sim \sum(|J_{nn}|^2 + |J_{nm}|^2) \equiv Tr(|J|^2)$. Meanwhile, since the trace $Tr(|J|^2)$ does not depend on the Aharonov-Bohm phase [11], G_j is weakly phase-dependent. This qualitative argument is confirmed by Fig. 4(d), where the calculated G_D and G_{ND} indeed have opposite phase variations, resulting in a weakly phase-dependent G_j. We note that the absolute value of G_j at any given phase is nevertheless finite.

To explain the strong G_j versus T, we rewrite G_{ND} in the continuous form [12]

$$G_{ND} = -\hbar\iint d\epsilon^+ d\epsilon^- \mathcal{C}(\epsilon^+, \epsilon^-)\mathcal{F}(\epsilon^+, \epsilon^-),$$
$$\mathcal{F}(\epsilon^+, \epsilon^-) = \frac{h\gamma}{(\epsilon^-)^2 + (h\gamma)^2}\frac{f(\epsilon^+ + \frac{\epsilon^-}{2}) - f(\epsilon^+ - \frac{\epsilon^-}{2})}{\epsilon^-}, \tag{5}$$

where ϵ^+ (or ϵ^-) is the average (or the difference) of two energy levels. $\mathcal{C}(\epsilon^+, \epsilon^-)$ is the current correlation function convoluting the DOS and $|J_{nm}|^2$ (for the full definition see [12]). It is illustrative to briefly examine the case of an unproximitized metal. Here, $G_D \equiv 0$ since $J_{nn} = \partial E_n/\partial\varphi \equiv 0$. For G_{ND}, since $\mathcal{C}(\epsilon^+, \epsilon^-)$ is constant in energy [12], Eq. (5) thus is reduced to the constant Drude conductance [12]. The situation is drastically different for the proximitized metal. From Eq. (5), an energy-dependent $\mathcal{C}(\epsilon^+, \epsilon^-)$ is essential for a temperature-dependent G_{ND}. At phase 0, the minigap fulfills such a requirement, resulting in $G_j \sim 1/T$ [7,9]. In our case, since G_j is weakly phase dependent, it is thus surprising that such $1/T$ dependence is true even at phase π where the minigap closes. To explain this, $\mathcal{C}(\epsilon^+, \epsilon^-)$ at phase π is shown in Fig. 4(b), with line cuts along $\epsilon^- = 0$ [Fig. 4(c)]. Although the DOS is indeed almost constant, a sharp peak in $\mathcal{C}$ appears at $\epsilon^+ = 0$ for a wide range of ϵ^-, revealing a strong current correlation between the ABSs far apart in energy but with electron-hole symmetry [21]. Approximating such peak as $\delta(\epsilon^+)$, $G_j = G_{ND}(\pi) \propto \int d\epsilon^- \mathcal{F}(0, \epsilon^-)$. Since $k_BT \gtrsim h\gamma$, we further have $G_j \sim \partial f/\partial\epsilon'(\epsilon' = 0) \sim 1/T$ as observed. $G_j \sim 1/T$ caused by the sharp peak in $\mathcal{C}$ at $\epsilon^+ = 0$ thus reveals a fundamental difference between a proximitized and an unproximitized metal, due to the electron-hole symmetry imposed by the superconductor. Finally, we note that the possibly temperature-dependent $\gamma(T)$ [11] does not cause the observed $G_j(T)$ in our parameter regime, as explained in [12].

Conclusion. In conclusion, we have measured the supercurrent noise and the linear admittance of a phase-biased SNS ring and verified the FDT long-predicted for the SNS junction. The junction conductance G_j is several times larger than the Drude conductance and follows a $1/T$ dependence. Using the linear response theory, $G_j \sim 1/T$ is a manifestation of the enhanced current correlation between the ABSs with electron-hole symmetry imposed by superconductors. While our results reveal the presence of the commonly overlooked dissipation source in the superconducting hybrid system, we further note that such a thermalization process is not restricted to the superconducting system but plays an important role in defining electrical conductance in generic phase-coherent conductors [23]. The supercurrent noise may

also be useful in detecting unconventional superconductivity [24–26] and unraveling decoherence channels in novel qubits [27,28]. Beyond superconductivity, our work is particularly relevant to systems such as mesoscopic normal rings which host persistent current [20,29], and more generally quantum materials with large orbital susceptibility [30–32]. In all these systems, as in the present experiment, the current with vanishing resistance may still exhibit significant thermal fluctuations.

Acknowledgments. We thank R. Weil, R. Delagrange, M. Aprili, and P. Simon for the discussions, L. Couraud and A. Cavanna for the development of HEMT, and A. Zobelli, E. Fayen, and J.-B. Touchais for help in using the cluster computation. This work received financial support by the French RENATECH network and by the European Research Council (ERC) under the European Unions Horizon 2020 research and innovation programme (grant Ballistop Agreement No. 833350).

[1] H. B. Callen and T. A. Welton, Irreversibility and generalized noise, Phys. Rev. **83**, 34 (1951).

[2] R. Kubo, The fluctuation-dissipation theorem, Rep. Prog. Phys. **29**, 255 (1966).

[3] D. Rogovin and D. J. Scalapino, Fluctuation phenomena in tunnel junctions, Ann. Phys. **86**, 1 (1974).

[4] D. A. Ivanov, R. von Roten, and G. Blatter, Minigap in a long disordered SNS junction: Analytical results, Phys. Rev. B **66**, 052507 (2002).

[5] H. le Sueur, P. Joyez, H. Pothier, C. Urbina, and D. Esteve, Phase controlled superconducting proximity effect probed by tunneling spectroscopy, Phys. Rev. Lett. **100**, 197002 (2008).

[6] D. Averin and H. T. Imam, Supercurrent noise in quantum point contacts, Phys. Rev. Lett. **76**, 3814 (1996).

[7] F. Zhou and B. Spivak, Resistance of superconductor-normal-metal-superconductor (SNS) junctions, J. Exp. Theor. Phys. Lett. **65**, 369 (1997).

[8] A. Martín-Rodero, A. L. Yeyati, and F. J. García-Vidal, Thermal noise in superconducting quantum point contacts, Phys. Rev. B **53**, R8891 (1996).

[9] P. Virtanen, F. S. Bergeret, J. C. Cuevas, and T. T. Heikkilä, Linear ac response of diffusive SNS junctions, Phys. Rev. B **83**, 144514 (2011).

[10] K. S. Tikhonov and M. V. Feigel'man, Admittance of a long diffusive SNS junction, Phys. Rev. B **91**, 054519 (2015).

[11] B. Dassonneville, A. Murani, M. Ferrier, S. Guéron, and H. Bouchiat, Coherence-enhanced phase-dependent dissipation in long SNS Josephson junctions: Revealing Andreev bound state dynamics, Phys. Rev. B **97**, 184505 (2018).

[12] See Supplemental Material at http://link.aps.org/supplemental/10.1103/PhysRevResearch.6.L022023 for the details of device fabrication, theoretical models, and data treatment.

[13] Y. Jin, Q. Dong, U. Gennser, L. Couraud, A. Cavanna, and C. Ulysse, Ultra-low noise CryoHEMTs for cryogenic high-impedance readout electronics: Results and applications, in *13th IEEE International Conference on Solid-State and Integrated Circuit Technology (ICSICT), Hangzhou, China, 2016* (IEEE, Piscataway, NJ, 2016), pp. 342–345.

[14] D. M. Pozar, *Microwave Engineering*, 4th ed. (Wiley, New York, 2011).

[15] M. Bonaldi, P. Falferi, M. Cerdonio, A. Vinante, R. Dolesi, and S. Vitale, Thermal noise in a high Q cryogenic resonator, Rev. Sci. Instrum. **70**, 1851 (1999).

[16] Z. Dou, T. Wakamura, P. Virtanen, N.-J. Wu, R. Deblock, S. Autier-Laurent, K. Watanabe, T. Taniguchi, S. Guéron, H. Bouchiat, and M. Ferrier, Microwave photoassisted dissipation and supercurrent of a phase-biased graphene-superconductor ring, Phys. Rev. Res. **3**, L032009 (2021).

[17] R. Haller, G. Fülöp, D. Indolese, J. Ridderbos, R. Kraft, L. Y. Cheung, J. H. Ungerer, K. Watanabe, T. Taniguchi, D. Beckmann, R. Danneau, P. Virtanen, and C. Schönenberger, Phase-dependent microwave response of a graphene Josephson junction, Phys. Rev. Res. **4**, 013198 (2022).

[18] R. E. Lake, J. Govenius, R. Kokkoniemi, K. Y. Tan, M. Partanen, P. Virtanen, and M. Möttönen, Microwave admittance of gold-palladium nanowires with proximity-induced superconductivity, Adv. Electron. Mater. **3**, 1600227 (2017).

[19] P. Dubos, H. Courtois, B. Pannetier, F. K. Wilhelm, A. D. Zaikin, and G. Schön, Josephson critical current in a long mesoscopic S-N-S junction, Phys. Rev. B **63**, 064502 (2001).

[20] N. Trivedi and D. A. Browne, Mesoscopic ring in a magnetic field: Reactive and dissipative response, Phys. Rev. B **38**, 9581 (1988).

[21] M. Ferrier, B. Dassonneville, S. Guéron, and H. Bouchiat, Phase-dependent Andreev spectrum in a diffusive SNS junction: Static and dynamic current response, Phys. Rev. B **88**, 174505 (2013).

[22] F. Zhou, P. Charlat, B. Spivak, and B. Pannetier, Density of states in superconductor-normal metal-superconductor junctions, J. Low Temp. Phys. **110**, 841 (1998).

[23] R. Landauer, Electrical transport in open and closed systems, Z. Phys. B **68**, 217 (1987).

[24] L. Fu and C. L. Kane, Josephson current and noise at a superconductor/quantum-spin-Hall-insulator/superconductor junction, Phys. Rev. B **79**, 161408(R) (2009).

[25] D. S. Shapiro, A. D. Mirlin, and A. Shnirman, Excess equilibrium noise in a topological sns junction between chiral Majorana liquids, Phys. Rev. B **98**, 245405 (2018).

[26] R. Seoane Souto, D. Kuzmanovski, and A. V. Balatsky, Signatures of odd-frequency pairing in the Josephson junction current noise, Phys. Rev. Res. **2**, 043193 (2020).

[27] A. Zazunov, V. S. Shumeiko, G. Wendin, and E. N. Bratus', Dynamics and phonon-induced decoherence of Andreev level qubit, Phys. Rev. B **71**, 214505 (2005).

[28] R. Harris, M. W. Johnson, S. Han, A. J. Berkley, J. Johansson, P. Bunyk, E. Ladizinsky, S. Govorkov, M. C. Thom, S. Uchaikin, B. Bumble, A. Fung, A. Kaul, A. Kleinsasser, M. H. S. Amin, and D. V. Averin, Probing noise in flux qubits via macroscopic resonant tunneling, Phys. Rev. Lett. **101**, 117003 (2008).

[29] M. Büttiker, Y. Imry, R. Landauer, and S. Pinhas, Generalized many-channel conductance formula with application to small rings, Phys. Rev. B **31**, 6207 (1985).

[30] J. Vallejo Bustamante, N. J. Wu, C. Fermon, M. Pannetier-Lecoeur, T. Wakamura, K. Watanabe, T. Taniguchi, T. Pellegrin, A. Bernard, S. Daddinounou, V. Bouchiat, S. Guéron, M. Ferrier, G. Montambaux, and H. Bouchiat, Detection of graphenes divergent orbital diamagnetism at the Dirac point, Science **374**, 1399 (2021).

[31] J. Liu, Z. Ma, J. Gao, and X. Dai, Quantum valley Hall effect, orbital magnetism, and anomalous Hall effect in twisted multilayer graphene systems, Phys. Rev. X **9**, 031021 (2019).

[32] D. Sticlet and J. Cayssol, Dynamical response of dissipative helical edge states, Phys. Rev. B **90**, 201303(R) (2014).